

<https://doi.org/10.1038/s43247-024-01390-y>

# Anthropogenic and atmospheric variability intensifies flash drought episodes in South Asia

Check for updates

Irfan Ullah<sup>1,2</sup>✉, Sourav Mukherjee<sup>3</sup>, Sidra Syed<sup>4</sup>, Ashok Kumar Mishra<sup>3,5</sup>, Brian Odhiambo Ayugi<sup>6</sup> & Saran Aadhar<sup>7,8</sup>

Flash droughts are abrupt and rapid intensification of droughts that affect agriculture, water, and ecosystems and are commonplace in South Asia. Despite their potential impact, flash drought evolution characteristics and underlying mechanisms in South Asia remain underexplored. We use a multivariate approach to analyze the onset speed, frequency, severity, duration, and return period of flash droughts, and the role of atmospheric circulation and human-induced climate change. We find that flash droughts are more common and intense in the crop season, especially in central India, western Pakistan, and eastern Afghanistan. They are caused by persistent atmospheric patterns that block moisture transport to South Asia. Additionally, anthropogenic climate change has intensified flash droughts in the spring-summer season, with a median fraction of attributable risk of 60%, 80%, and 90% for Afghanistan, Pakistan, and India, respectively. Our results suggest that flash droughts will expand and worsen in the future, requiring adaptation measures for the water, agriculture, and energy sectors.

Droughts are the most multifaceted and complex among all extreme weather events, driven by natural climate variability and anthropogenic influence<sup>1–3</sup>. Drought events usually evolve slowly over a large geographical area triggered by a combination of meteorological conditions (e.g., reduced precipitation and higher temperature) over an extended period, resulting in substantial impacts on water, agriculture, energy, and environmental sectors and socio-economic conditions<sup>4–6</sup>. Compared to traditional droughts, flash droughts (FDs) are categorized by their sudden onset and rapid intensification over a short period, persisting over a few weeks to months<sup>7</sup>. In the recent past, FD research has garnered much interest from the scientific community, particularly after the occurrence of severe FDs in Australia<sup>8</sup>, South China<sup>9</sup>, the Central United States<sup>10,11</sup>, and many other parts of the globe<sup>12–17</sup>.

Due to the lack of appropriate tools for robust quantification and prediction of FDs, such events are a major concern for stakeholders. Besides, FDs can trigger compound extreme events (e.g., heatwaves and wildfires), leading to increased risks to water and food security and environmental sustainability<sup>15,18–20</sup>. Due to the multivariate nature of FDs<sup>21,22</sup>, their impacts

are compounding in nature. Thus, it is necessary to explore the multivariate risk from FD using the nuance probabilistic framework and explore its underlying causes (a physical mechanism) in a changing climate.

FDs have been studied in several global hotspots experiencing amplified risks<sup>23</sup>; however, most studies are limited to exploring the causes and consequences of FDs caused by meteorological drivers<sup>9,24–26</sup>. A recent study investigated the evolution of FDs in Spain and the underlying meteorological drivers over the last six decades and suggested that FDs are mainly attributed to water-scarce regions during the summer season<sup>27</sup>. While many studies investigated FDs in different parts of the world, this study further complements and advances previous research in several ways, as discussed hereafter. Firstly, the rapid FD onset phase and associated causes with hydrometeorological factors are limited<sup>9,28–31</sup>, and the transition in FD characteristics between consecutive seasons driven by changes in seasonal climate is not explored. Secondly, regional extreme events are usually influenced by large-scale atmospheric variability that can potentially alter the FDs onset, i.e., land–atmospheric interactions and monsoon processes<sup>13,14,32–34</sup>, which remain underexplored. Such processes affect the

<sup>1</sup>College of Hydrology and Water Resources, Hohai University, Nanjing 210098, China. <sup>2</sup>China Meteorological Administration Hydro-Meteorology Key Laboratory, Hohai University, Nanjing 210098, China. <sup>3</sup>Center for Forested Wetlands Research, Southern Research Station, USDA Forest Service, 3734 Highway 402, Cordesville, SC 29434, USA. <sup>4</sup>Institute of Peace and Conflicts Studies, University of Peshawar, 25000 Peshawar, Pakistan. <sup>5</sup>Zachry Department of Civil & Environmental Engineering, Texas A&M University, College Station, TX, USA. <sup>6</sup>Department of Civil Engineering, Seoul National University of Science and Technology, Seoul 01811, Republic of Korea. <sup>7</sup>Civil and Infrastructure Engineering, Indian Institute of Technology (IIT), Jodhpur, India. <sup>8</sup>Centre for Intelligent Infrastructure, IIT Jodhpur, Jodhpur, India. ✉e-mail: [Irfan.marwat@hhu.edu.cn](mailto:Irfan.marwat@hhu.edu.cn)

occurrence of FDs as well as climate characteristics and have been evident across the globe<sup>22</sup>. Different evaporation regimes have distinct surface energy partitioning depending on the energy-limited and water-limited conditions<sup>35</sup>. More specifically, although the local scale moisture balance of the land-surface can govern FD intensification, these processes depend on the type of evaporation regime. For example, the positive feedback loop between evaporative demand and evaporation is common in energy-limited conditions when water availability is not a limiting factor for evaporation. However, the evaporation rate and the evaporative demand diverge in water-limited conditions due to a prolonged state of available moisture deficit. This leads to an increase in sensible heat flux instead of evaporation (decrease in latent heat flux), which increases near-surface air temperature and vapor pressure deficit, thus facilitating the development of FD events<sup>14</sup>. Recently, few studies have investigated the potential role of summer monsoon failure on drought occurrences in South Asia (SA)<sup>13,16,36,37</sup>. These studies highlighted the important implications for understanding the prospective role of large-scale atmospheric variability on the onset speed of FDs during spring-summer transition seasons in the world's densely populated regions, like SA. However, none of the studies explores the changes in FD's onset speed and intensity and the possible role of anthropogenic climate change in altering the risk of FD across SA.

Southwestern SA experienced a fast transition from a non-drought state to a severe drought state within a transition season<sup>38,39</sup>. Extreme climatic conditions are likely to upsurge in SA by the end of the 21<sup>st</sup> century<sup>13,40–42</sup>. For example, an extreme FD event occurred unexpectedly in late spring of 2022 across Pakistan in southwestern SA and continued throughout the summer<sup>43</sup>. The unprecedented speed at which the spring-summer FD began raises questions about whether such an extraordinary event will be a new normal in a warmer climate<sup>13</sup> or whether climate change is a crucial driver in the rapid intensification of drought. Therefore, in-depth attribution analysis is essential to quantify the speed and occurrence of FD development, which has far-reaching implications for developing an early warning system for hotspot regions in SA. It is expected that extremely hot and dry spells that cause FDs may occur more frequently due to changing climates<sup>34</sup>. Yet, anthropogenic risk on FDs associated with potential land-atmospheric interaction is less recognized compared to conventional droughts<sup>44,45</sup>.

Considering these existing knowledge gaps, our objective is to investigate the characteristics of FD evolution using a multivariate probabilistic approach and explore the potential role of atmospheric circulations associated with them. In the present study, we examine the occurrence of FDs, associated multivariate recurrence intervals, and the influence of atmospheric circulation variability and anthropogenic climate change on FDs over the SA region. A bivariate modeling framework was used to quantify the joint return periods (JRPs) of a FD severity and duration. Under different climatic forcing's, CMIP6 simulations were used to attribute and identify the effect of anthropogenic climate change on FD intensity and onset speed over SA. The results from this study will help prioritize adaptive measures to reduce and mitigate the impact of FDs.

## Results

### Flash drought features in South Asia

The onset and termination of FD information are crucial factors to minimize their impact on the agricultural sector, which can drastically reduce crop yields, cause significant economic losses, and threaten food security. Figure 1a, b and Supplementary Fig. 3 show the spatial distributions of FD frequency, severity, and duration across SA, especially in agriculturally important regions (Supplementary Fig. 1). Figure 1c shows the annual variation of regional FD frequency for the Spring-summer and summer season. The FD events in each SA region were examined by the season (Spring-summer and summer) in which rapid drought development evolved.

A modified Mann–Kendall trend test was performed for the period 1979–2021 to investigate whether statistically significant trends exist in monthly FD severity, frequency (shown in Fig. 1a, b, and Supplementary

Fig. 2a, b), and duration (shown in Supplementary Fig. 3a, b) for both the spring-summer and summer season in South Asia. Results show that the majority of the subtropics and semi-arid regions exhibit relatively higher FD frequency compared to other regions within the growing season during the period 1979–2021. This can be noted for central India, western Pakistan, eastern Afghanistan, Bangladesh and Nepal for the spring to summer transition seasons during the period 1979–2021 (Fig. 1a). Simultaneous occurrences of FD onset are evident for India and Pakistan, with highest in FD frequency during summer. Weakened mid-latitude synoptic disturbances suppress frontal activities before the monsoon onset in SA and connected regions (south China), facilitating the drying trend<sup>46</sup>. This may lead to precipitation variability and a notable drying trend prior to the monsoon onset, leading to a more abrupt thus amplified FD over SA during the spring-summer season. However, the severity and duration of FD in Afghanistan and Bangladesh are generally less determined during the growing season (Fig. 1b and Supplementary Fig. 4). For central-southern India and northern Pakistan regions, the FD frequency distribution varies from the major seasonal variability exhibited in northern India and the Himalayan foothills, i.e., FD frequency peaks in the late spring and early summer (Supplementary Fig. 4). For instance, in northern and central SA, the highest annual variability of FD frequency is exhibited across agriculture-dominant regions. At the same time, southern SA observed the highest FD frequency before the end of the Kharif growing season.

The variation of the annual mean FD frequency time series during the spring-summer and summer seasons across SA countries are presented in Fig. 1c. From the time series results, it is clear that the FD frequency for the spring-summer season increased significantly (at 95% confidence level) by about 20%, 40%, 60%, and 80% across Sri Lanka, Afghanistan, Pakistan, and India during the recent two decades (e.g., 2000–2020). In addition, compared to the summer season, the spring-summer transition season shows a higher rate of increase in FD frequency which is indicated by the greater magnitude of slope (per year) of the trend line for all regions during the spring-summer transition season. However, relatively less frequent but consistent variation of FD frequency for both the spring-summer and summer seasons was exhibited for Nepal, Bhutan, and Bangladesh with an amount of 20% to 30%, especially during the 1980–1990 and 2000–2020 periods. The FD frequency continued to exacerbate significantly throughout the spring-summer and summer transition seasons across the regions particularly in the recent decade (2010–2020). From 2010 onwards, FD duration in Sri Lanka, Afghanistan, Pakistan, and India was exacerbated, and the severity became more intensified (Supplementary Figs. 2 and 3). This trend continued throughout the spring-summer transition season; by 2020, the average FD frequently exceeded up to 70% for the above-mentioned regions. For example, in Pakistan and India, FD's frequency and severity persisted throughout the early 2010 summer, which intensified from 2020 onwards during the spring-summer season.

### Areal extent and hydrometeorological anomalies

Figure 2a shows the median of the largest FD areas for the spring-summer and summer seasons, while Fig. 2b indicates the standardized interannual variations of average precipitation, temperature, soil moisture, and evapotranspiration anomalies across SA during the period 1979–2021. The probability density plots in Fig. 2a indicates a considerable increase in the probability of larger FD-affected area in the spring-summer transition season relative to the summer season during the period 1979–2021. Notably, there is a substantial shift of 7% in the median of the distribution of FD-affected area of the SA landmasses from 17% during the summer season to 24% during the spring-summer transition season.

To further explore the evolution of FD events, we derived the seasonal anomalies of total precipitation, mean temperature, mean evapotranspiration, and soil moisture time series across FD-affected land areas during 1979–2021 (Fig. 2b). We observed that abruptly higher than usual temperature, reduced precipitation, and high evapotranspiration frequently accord a high percentage of FD-affected landmasses. The percentage of FD-affected landmasses during the spring-summer season ranks higher than the

summer season during 1979–2021. Most regions are accompanied by a warm temperature anomaly, high evapotranspiration, limited soil moisture, and a precipitation deficit. The greater percentage of land areas are accompanied by extreme temperatures and limited soil moisture due to precipitation deficits. Elevated temperatures, high evapotranspiration, and a severe precipitation deficit could facilitate FD which leads to the rapid decline in the soil moisture triggering FDs' onset<sup>34</sup>. Temperature and precipitation are the key components influencing the FD evolution, which alternately leads to the rapid decline in the soil moisture triggering FDs' severity.

**Joint return period of flash drought events**

Figure 3 elucidates the joint return period and linear association of FD events. In terms of two-dimensional relationships (Fig. 3a), the majority of the FD events were found in the range (95% confidence interval) of the linear model. These ranges for FD duration were smaller (narrower) than those for severity, suggesting that the significance of FD duration for the accumulative influence of drought onset was greater than that of severity. Moreover, south-central India, western Pakistan, and eastern Afghanistan had a statistically substantial increasing trend ( $p < 0.1$ ) in FD severity

(Fig. 1b). In contrast, the rest of the regions, Nepal, Bhutan, Bangladesh, and Sri Lanka showed a statistically noteworthy declining trend ( $p < 0.1$ ), respectively. Besides, the magnitude of the trend varies across regions. For instance, statistically significant trends in severity across southern Pakistan, northern Afghanistan, and central Afghanistan were exhibited with very modest changes (~30%) in the spatial coverage of FDs during the study period. It is important to note that the mean FD durations in south-central India and southern Pakistan are about 20–80 days and 20–60 days, followed by those in northern Afghanistan and central Bangladesh at about 15–25 days and 20–50 days, implying a considerable drought impact in terms of intensification. In contrast, similar spatial patterns were exhibited for changes in frequency and severity as compared to duration (Supplementary Figs. 2 and 4), where south-central SA had more frequent FD events with longer durations throughout the study period.

The JRP of the FD events is calculated based on the event's severity and duration within a bivariate copula framework (Fig. 3a, b). The JRP of FD events for the spring-summer and summer seasons are calculated individually to study the potential influence of transitional seasons on the FD severity and duration. The FD events tend to be more frequent during the summer than the spring-summer season based on the higher number of FD

**Fig. 1 | Flash drought features during the spring-summer and summer season in South Asia.**

**a, b** Spatial maps show the monthly mean of (a) FD frequency (%), and (b) FD severity (%) for spring-summer transition season. In Fig. 1b, the black dots indicate the locations with statistically significant trends (at a 5% significance level), determined using the modified Mann–Kendall trend test. **c** Time series plots presenting the annual variation of FD frequency (%) during the spring-summer and summer seasons across SA countries.

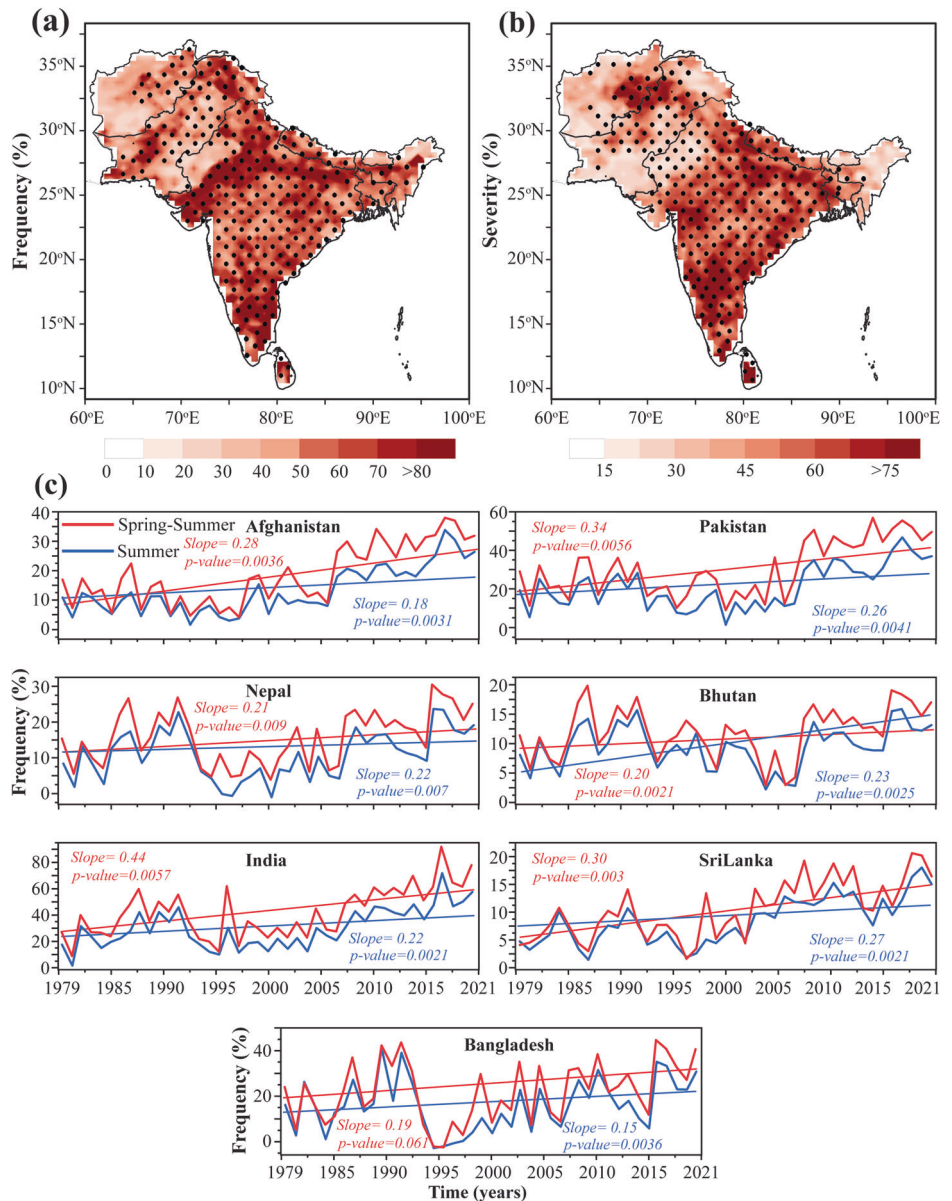
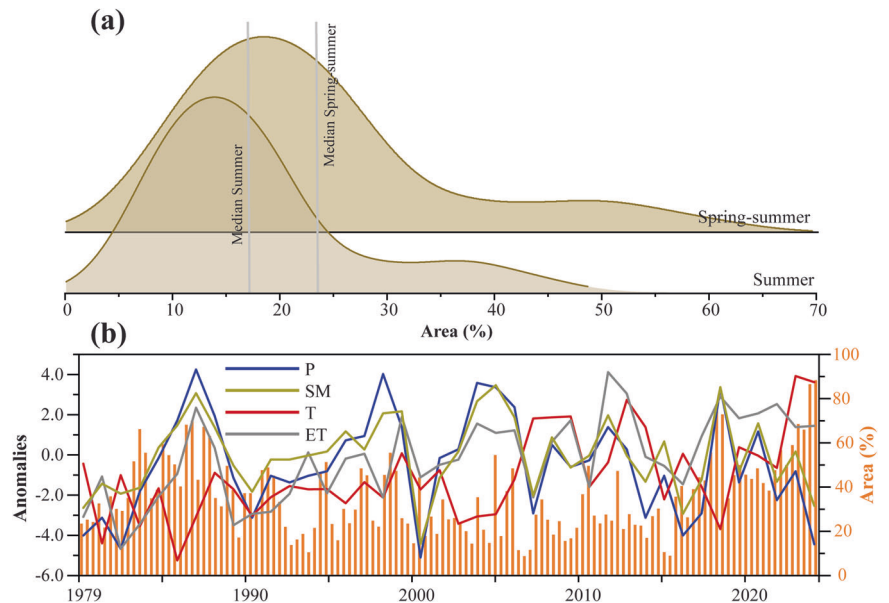


**Fig. 2 | FD-affected area and the time series of anomalies for selected hydrometeorological variables. a** Probability distribution functions of the largest FD area (percentage) estimated for the spring-summer season and summer season for the 1979–2021 period. Note that the vertical solid lines (in gray) indicate the median values of the FD-affected area for the spring-summer and summer seasons. **b** Indicates interannual variations of the standardized spring-summer mean precipitation (P: blue), soil moisture (SM: brass), temperature (T: red), and evapotranspiration (ET: gray) anomalies averaged (right y-axis) and the proportion of land affected by FD for each year (left y-axis) over South Asia during the 1979–2021 period.



events exhibiting a JRP of less than 5 years. However, the FD events in the summer season are characterized by less severity with a duration of less than a few weeks, compared to the spring-summer season. The results reveal that the spring-summer season experienced more severe and longer FD events relative to the summer season (Fig. 3a). The most severe FD occurred during the spring-summer transition season and had a JRP between 50 and 100-year lasted for 60 days with a severity of 20.5. On the other hand, during the summer season (Fig. 3b), the most severe FD event had a 50 to 100-year event lasting 45 days and had a severity of 15.5. Overall, the results from the analysis indicate the multiple adverse effects of FD in the SA region and their strong dependence on seasonality.

**Potential role of anthropogenic climate change**

We calculated the fractional attributable risk (FAR) to investigate the potential role of anthropogenic climate change on the spring-summer season FD events. The attribution analysis was performed using the CMIP6 model outputs under NAT and ALL external forcings by considering ALL as factual and NAT as the counterfactual climate scenario. A grid cell-based analysis was performed to calculate the FAR based on the comparison of changes in soil moisture percentiles (spring minus summer) in the ALL, relative to the NAT scenario (see Methods). The spatial distribution of FAR is demonstrated by the boxplots depicted for the selected countries located within the SA region (Fig. 4b). We used the student’s t-test to determine if the change in FD onset speed in the ALL scenario is significantly different (at 5% significance level) from that in the NAT scenario. The spatial distribution of the FAR suggests that anthropogenic influence will likely amplify the risk of increased spring-summer FD onset speed in the SA region. For example, the median FAR for the spring-summer event across Afghanistan, Pakistan, and India is estimated to be 60%, 80%, and 90% (Fig. 4a, b), respectively. The FAR for Nepal, Sri Lanka, and Bangladesh are close to the median values of 45%, 55%, and 65%, respectively.

Additionally, we investigated the statistical shift in the median values and the statistical similarity/dissimilarities of the family of the distribution of the grid-cell-based changes in severity of FD onset speed between the NAT to the ALL scenario based on each country, as shown in Fig. 4c. Non-parametric Kernel probability density was estimated using the grid-cell values of the changes in soil moisture percentile for different countries located within the SA region. To test whether the shift in median among the NAT and ALL scenarios is statistically significant at a 5% significance level, we applied the Wilcoxon rank-sum (WR) test. Additionally, we tested whether the FD onset speed for the NAT and ALL scenarios comes from a different family of distribution using the two-sample Kolmogorov-Smirnov

(KS) test. The results from the WR and KS test, and the probability density estimates suggest that the spatial distribution of the FD onset speed across Afghanistan, Pakistan, India, and Bangladesh exhibit a statistically significant (at a 5% significance level) positive shift in the median and overall distribution in the ALL scenario compared to the NAT scenario. This indicates a significant influence of anthropogenic climate change in amplifying the FD onset speed during the spring-summer season in the SA region. This highlights the prerequisite to understanding rapid anthropogenic encroachment triggering rapid intensification of FD events across these regions that could result in underestimation of the FD event risk, leading to inadequate policy responses. Our findings underscore the potential impact of climate change on FD risk, and the need to prioritize proper adaptation actions in each country to mitigate the adverse impacts of FD events.

**Physical processes that influence flash droughts**

To investigate the physical processes of FD development, anomalous atmospheric circulation patterns were examined for the spring-summer season (March–August) and summer (June–August) across SA during 1979–2021. Monthly mean anomalies for geopotential height 500-hPa (shaded) and winds 850-hPa (vector), 2 m air-temperature, mean sea level pressure, specific humidity, 500-hPa vertical velocity for the spring-summer season and summer season, relative to the 1979–2021 climatology are calculated for the target region, as shown in Fig. 5.

During spring-summer (Fig. 5a), a dipolar pressure system is prominent between the eastern and western edges of the target region. While negative geopotential height anomalies are prominent on the eastern edge, positive geopotential height anomalies dominate on the SA western edge. This dipolar system can actively promote an adiabatic wind and pressure gradient, greater condensation, and a precipitation deficit in the region. However, the synoptic system is considerably different during the summer season. Negative geopotential height anomalies persist in the western edge, signifying a low-pressure system in place, resulting in a precipitation deficit over the region (Fig. 5b). A similar distribution can be observed for specific humidity and mean sea level pressure during the spring-summer season (Fig. 5c), while higher air temperature anomalies appear over eastern parts of the SA. A combination of greater relative humidity and higher air temperature, higher cloud liquid water content can be noted over western SA, including Afghanistan and Pakistan, signifying increased precipitation (Supplementary Fig. 5). The enhanced mean sea level pressure further enhances the role of the sub-tropical and Somali jet streams, suggesting that the primary drivers of oceanic water transport to continental landmasses

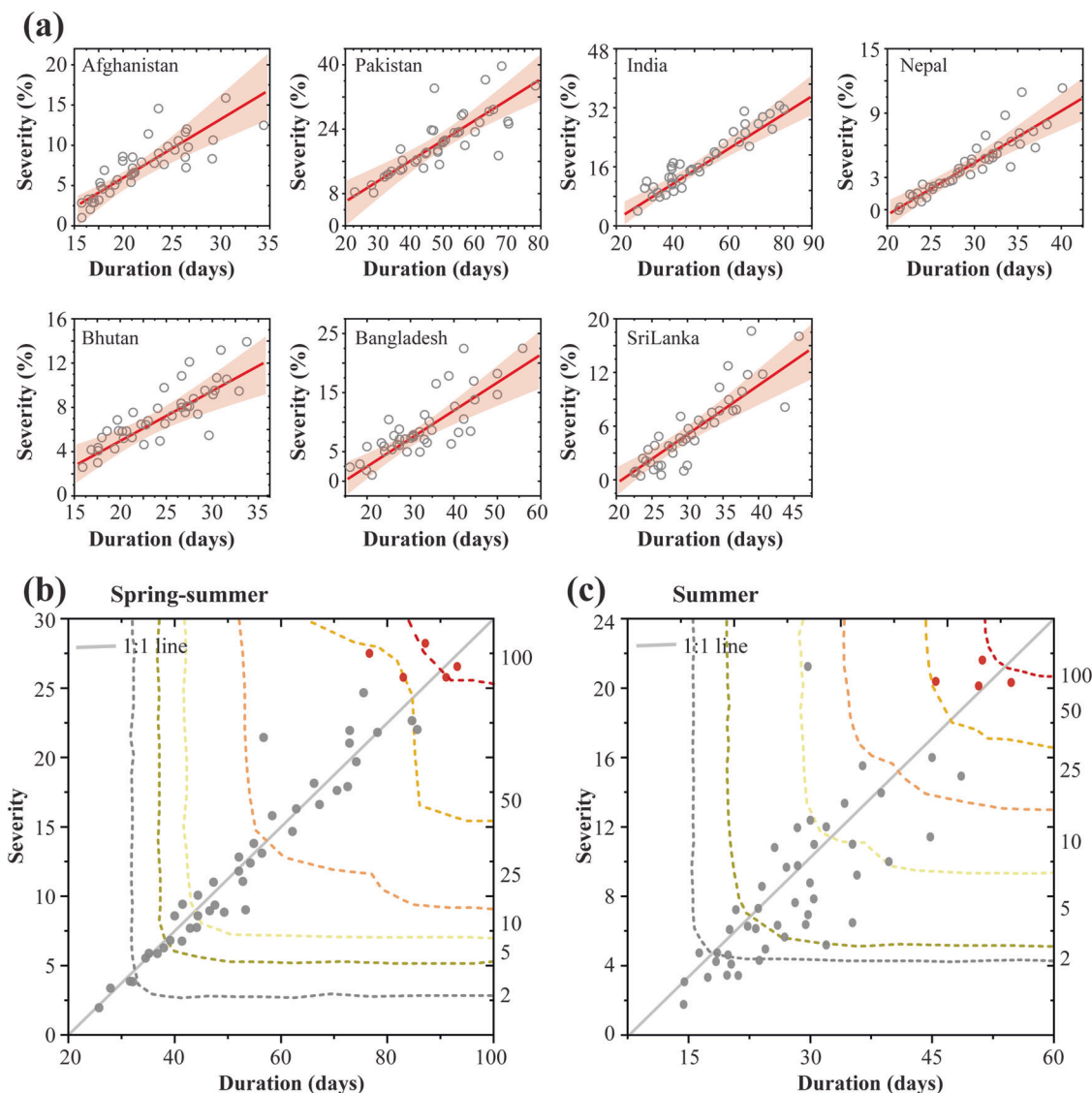


**Fig. 3 | Linear association and joint return period of flash drought duration and severity.** **a** The upper panels show the linear relationship between FD duration and severity for different countries of SA, where the light red line denotes the predicted band at the 95% CI of the sample based on their model relationship. **b** The joint return period between FD duration and severity for the spring-summer (March–

August), is same for the (c) but for the summer season (June–August). The red dots indicate the most severe FD events that occurred during the historical period, 1979–2018. The short-dashed lines denote the JRP (i.e., 2, 5, 10, 25, 50, and 100-year) of the events.

determine the precipitation pattern across the summer monsoon-dominant regions (Fig. 5d). However, higher temperatures with no or fewer changes in precipitation and increased relative humidity further facilitates the drier conditions over the SA region (Fig. 5c, d). Conversely, increasing vertical velocity anomalies dominate in the western parts due to high air temperatures, while decreasing anomalies appear in the eastern parts of the study area as well as over the Bay of Bengal (BoB; Fig. 5e). Similar patterns were exhibited during the summer season when low-pressure systems migrated westward with depressed air temperatures and, as a result, created negative vertical velocity anomalies (Fig. 5f).

Overall, based on these findings, it can be concluded that the convergence of the cloud liquid water contents and increased relative humidity from both easterlies and south-westerlies altogether result in warm episodes, which are even more amplified when the easterlies through the BoB are stronger. Conversely, the continental landmass of SA is characterized by a strong anticyclonic trend related to decreasing winds and less precipitation. The anticyclonic trend appears to push cyclonic movement near the tropics and the northern sections of the Bay of Bengal (BoB). Nevertheless, due to the regional precipitation dependence on moisture/water vapor, it can be

noted that the anomalous wind pattern leads to precipitation variability. Thus, relatively strong air temperature gradients appear in the Arabian Sea triggered by the difference in positive and negative anomalies in SST. These enhanced air temperature gradients in the Arabian Sea are stronger throughout the spring-summer season than in the summer (see Supplementary Fig. 5). In contrast, during the spring-summer transition season, FD event onset may be triggered by the inhibition of convection and reduced land-ocean thermal gradient caused by the persistent and stationary anticyclonic system facilitated by negative temperature anomalies over the Indian Ocean and the adjacent air aloft.

### Discussion

This study systematically explores the hotspot regions for FD evolution and the effects of anthropogenic climate change and physical mechanisms during the spring-summer season across SA for the period 1979–2021. Specifically, we investigated the onset and speed of FDs, their associated recurrence intervals based on a multivariate framework, the influence of hydroclimatic anomalies, atmospheric circulation variability, and the potential influence of anthropogenic climate change using the reanalysis

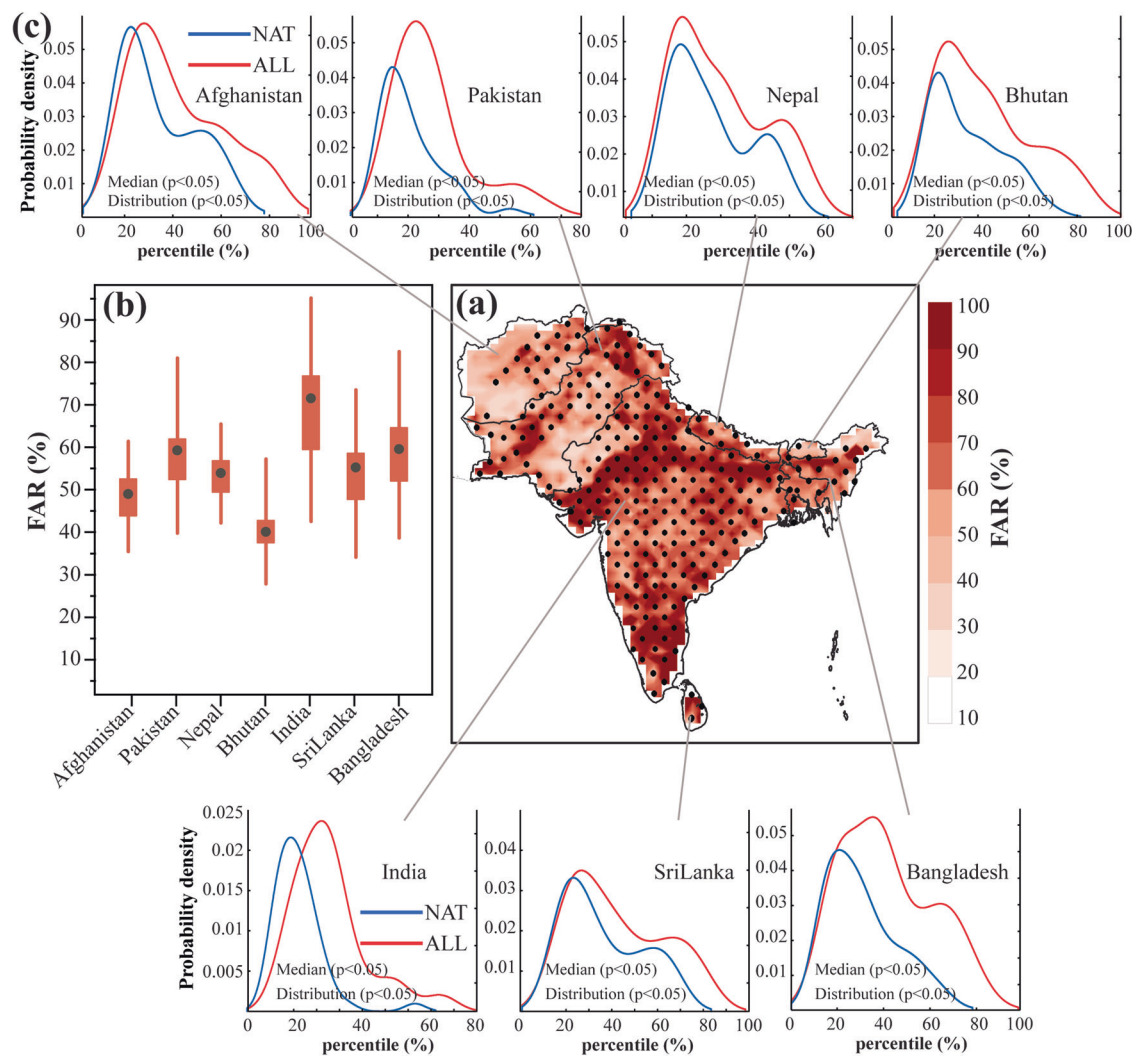


**Fig. 4 | Potential role of anthropogenic climate change.** **aa** Spatial distribution of FAR (%) of change in FD onset speed, across South Asia. The black dots in (a) indicate the grid cells where the change in onset speed of FD in the ALL scenario is significantly different (at a 5% significance level) from that in the NAT scenario, determined using the student's *t*-test. **b** Box and whisker plots represent the median and interquartile range for their corresponding country-wise FAR (%). **c** Probability density estimates of multi-model ensemble mean of soil moisture percentiles for the

ALL (red) and NAT (blue) scenarios indicate the change in FD onset speed for each country within the SA region. Note that the change in onset speed is estimated as the difference in the mean soil moisture percentile between the spring and summer seasons (spring minus summer). The hypothesis testing of the same distribution family and median (as shown in c) is performed using the Kolmogorov-Smirnov, and rank-sum significance test, respectively.

and outputs from CMIP6 GCMs. A copulas-based bivariate modeling framework was employed to quantify the JRP of the FD's severity and duration. We found that most of the regions exhibit increased FD frequency within the growing season (between spring and summer) for central India, western Pakistan, and eastern Afghanistan, followed by Bangladesh and Nepal. In terms of joint distributions, India and Pakistan revealed the highest FD frequency during summer. In contrast, the severity and duration of FD in Afghanistan and Bangladesh are generally fewer but intense throughout the growing season, which is consistent with the outcomes of earlier studies<sup>13,16</sup>. In addition, south-central India, western Pakistan, and eastern Afghanistan had a statistically substantial increasing trend in FD severity, implying the dominance of the exacerbated soil moisture depletion across those regions<sup>13,16,17,47</sup>.

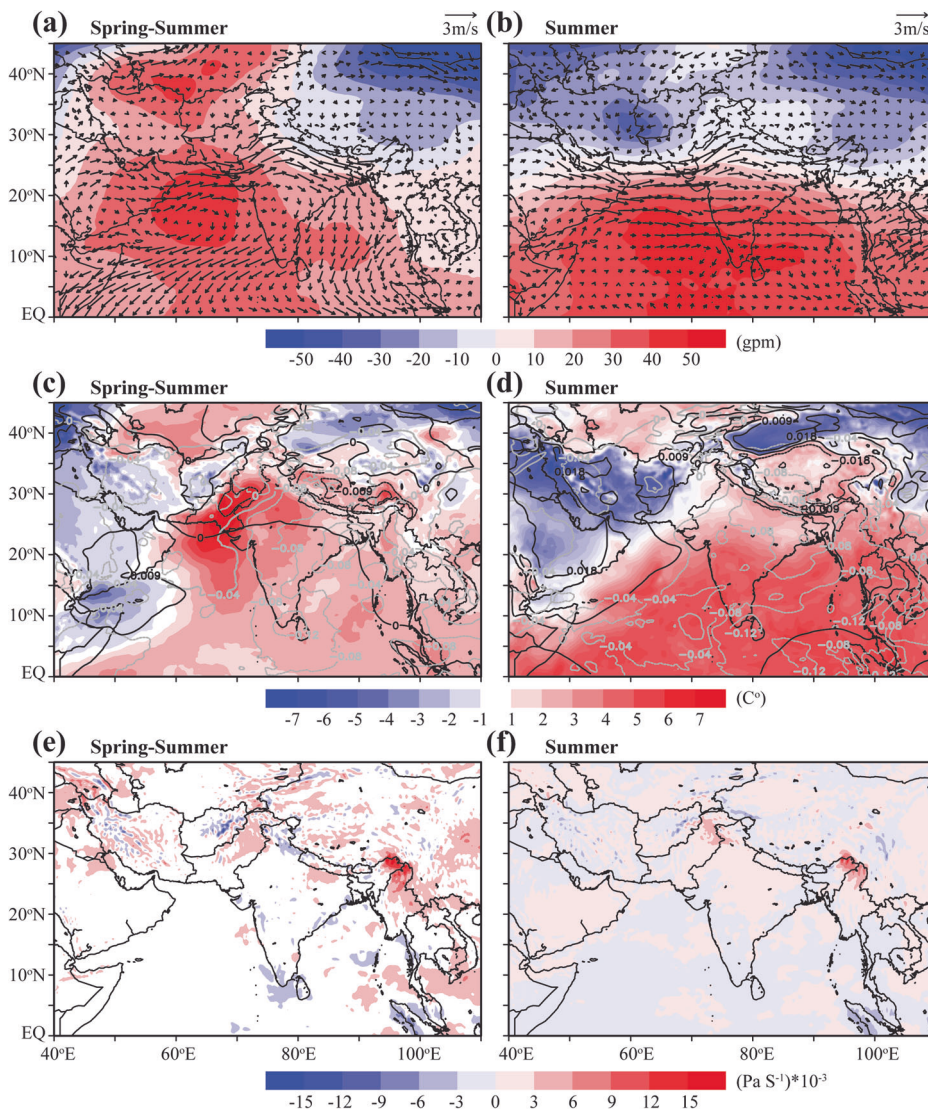
The median of the FD-affected area increased from 24% of the SA landmasses during the spring-summer season to 17% in the summer season. The warmer climates resulted in drier conditions and postulated that drought would occur more frequently and last longer<sup>48</sup>, even though without specific attribution studies. It is worth noting that the mean FD durations in south-central India and southern Pakistan are about 20–60 days, inferring a

rational drought impact in terms of intensification. In this study's findings, the FD duration for most of the regions lasted more than a week. A reasonable impact of short-lived flash drought could possibly be on vegetation productivity which is expected to exacerbate in a warming future. It is mainly because FD develops more rapidly with higher temperatures, which is why the ecosystem may not have enough time to adapt to the sudden onset of large water deficits coupled with heat extremes, resulting in a rapid reduction in ecosystem productivity<sup>16</sup>. Previous studies have also shown a higher FD risk across central India and Pakistan<sup>17,22,49</sup>. The findings from the study also suggest that a larger proportion of FD event occurrences, characterized by a JRP of 5 years or less are less severe and last less than a week during the summer season as compared to the FD event in the spring-summer season. Additionally, the most severe FD recorded in the spring-summer had a JRP of between 50 and 100 years that lasted for 70 days and had a severity of 25.5. On the other hand, the most severe FD recorded in the summer season was a JRP of 50 to 100-year events that lasted for 50 days and had a severity of 15.5.

This study also pays close attention to the relevant physical mechanisms as potential drivers that may cause the rapid onset of FDs. The summer

**Fig. 5 | Spatiotemporal evolution of monthly mean anomalies of meteorological forcing for the spring-summer season and summer season.**

**a, b** Spatial map showing the 500-hPa geopotential height anomalies (shaded) and 850-hPa wind (vector) anomalies relative to the 1979–2021 climatology for the spring-summer and summer seasons. **c, d** indicates 2 m temperature anomalies (shading), specific humidity anomalies (shown by gray dashed contours), and mean sea level pressure anomalies (indicated by solid black contours). **e, f** showing the 500-hPa vertical velocity (shaded) for the spring-summer and summer seasons across the SA region.



monsoon precipitation is the major cause of surface water availability in many parts of SA; however, it is well-known that the drought's onset in SA is well-interrelated with the summer monsoon failure<sup>13,32,50,51</sup>. Besides, SST plays a mediating role in compensating the spring soil moisture effect of summer East Asian monsoon precipitation with reduced precipitation under negative or positive SST backgrounds, promoting decreasing the spatial extent of precipitation anomalies<sup>52–56</sup>. Our results reveal a dipolar pressure system with positive geopotential height anomalies on the eastern edge and negative geopotential height anomalies on the western edge of the target region during the spring-summer season, promoting adiabatic wind gradient, enriched condensation, and thereby, a precipitation deficit in the region. Conversely, the summer season exhibited low-pressure systems that migrated westward during the spring-summer with depressed air temperatures and, as a result, created negative vertical velocity anomalies. In general, the continental landmass of SA is attributed to a strong anticyclonic trend, which is related to decreasing winds and less precipitation in the northern hemisphere. Interestingly, relatively rich air temperature gradients appeared in the Arabian Sea due to positive and negative anomalies in SST, particularly in spring-summer. In contrast, negative temperature anomalies and the adjacent air upward over the Indian Ocean show a constant atmosphere with stationary perseverance impeding convection and reducing the land-ocean thermal gradient. Our findings are consistent with<sup>52</sup>, that spring soil moisture potentially affects the summer East Asian monsoon precipitation, and<sup>13</sup>, who further reported that anticipated FDs rise is

primarily allied with the rapid failure in soil moisture, especially in the late summer monsoon season.

Our results suggest that the FD's rapid onset can be accredited to large-scale atmospheric drivers and land-atmosphere feedback, which is the key factor of FDs with respect to anthropogenic climate change. The preferential FD occurrence could be attributed to several factors across SA hotspot regions; however, the role of physical drivers is significantly noted for the development of FD<sup>17,49,57</sup>. Large-scale atmospheric drivers influence the regional moisture imbalance and thermal variables by altering the regional temperature, precipitation, and evapotranspiration. The combination of anomalous variables (temperature, precipitation, soil moisture, and evapotranspiration) that arise concurrently may cause the FD's rapid onset across many regions of SA. Further scope of research can be investigating the joint role of these large-scale meteorological contributions and the local cascading association between drought and heat extremes<sup>58</sup> that can lead to increased frequency of FD onsets.

The results from attribution analysis suggest a significant influence of anthropogenic climate change on the increased onset speed of FD events in the spring-summer transition season. For instance, the median FAR for the onset speed of spring-summer FD events in Afghanistan, Pakistan, and India is 60%, 80%, and 90%, respectively (Fig. 4a, b). On the other hand, the median values of the FAR for Nepal, Sri Lanka, and Bangladesh are 45%, 55%, and 65%, respectively. The spatial variability of FAR may arise due to the uncertainty in hydro-meteorological changes over the water-energy-

limited regions under global warming<sup>59</sup>. In addition, not only the mean of the total column soil moisture but also the variability across the vertical column of the soil moisture captures a more holistic dynamics of the soil moisture variation. However, in this study, we focused on the temporal dynamics of the mean state of the vertical soil moisture profile during flash drought which may be another limitation of this study<sup>23,60–62</sup>.

Overall, the study findings can help climate change institutions, policymakers, and practitioners at the country level to target anthropogenic interventions to regions and communities that are most at risk of FD events, and to adapt their policies to the explicit needs and features of different climatic regions and populations. Our results support the finding of<sup>9</sup>, who found that the 2019 FD intensity and onset speed in southern China are accelerated by anthropogenic climate change. Besides, we assess the changes in bivariate risks using a copula modeling framework, which reveals higher risks than recent studies across SA<sup>13,36</sup>. Identifying the FD drivers and the related components that may accelerate the rapid failure in soil moisture is essential to developing credible risk reduction strategies based on multivariate contexts across varied climate and environmental conditions. Not only the mean of the total column soil moisture but also the variability across the vertical column of the soil moisture captures a more holistic dynamics of the soil moisture variation<sup>63</sup>. However, in this study, we focused on the temporal dynamics of the mean state of the soil moisture during flash drought. More specifically, we only focused on exploring the inter-scenario comparison of the mean soil moisture state during flash drought episodes at any given location but across the two seasons. The attribution study henceforth follows the same underlying assumption. Thus, more in-depth studies are required to advance our understanding of FD evolution and how these events impact environmental, social, and socio-economic sectors in different parts of the world.

## Materials and methods

### Datasets

This study uses hourly root-zone soil moisture products acquired for the three layers, i.e., layer 1: 0–7 cm, layer 2: 7–28 cm, and layer 3: 28–100 cm, and other daily parameters such as precipitation, surface air temperature, and evapotranspiration obtained from the European Center for Medium-Range Weather Forecasts Reanalysis 5 (ERA5, Copernicus Climate Change Service [C3S])<sup>64</sup>. The hourly datasets were averaged over a common epoch of 1979–2021 across the native and uniform grids of  $0.25^\circ \times 0.25^\circ$  horizontal resolution. To examine the physical causes of the SA FD events, we derived monthly datasets of 500-hPa geopotential height, 850-hPa wind, 2 m temperature, sea surface temperature (SST), specific humidity, mean sea level pressure, cloud liquid water content, and 500-hPa vertical velocity from ERA5 for the same spatial and temporal coverage. The attribution analysis was performed using monthly full-column mean soil moisture, temperature, precipitation, evapotranspiration, and SST outputs from 10 atmosphere-ocean coupled general circulation models (GCMs) provided by the Coupled Model Intercomparison Project Phase 6 (CMIP6)<sup>65</sup> at  $0.25^\circ \times 0.25^\circ$  (Supplementary Table. 1). The CMIP6 model simulations capture both forcing (the combination of ALL simulations from 1979–2014 and “middle of the road” scenarios (SSP245; 2015–2021)) and natural forcing (NAT simulations from 1979–2021). During attribution analysis, full-column soil moisture products are processed into percentiles<sup>9</sup> due to different soil depths in CMIP6 models for a fair comparison among models and across regions. ALL simulations were driven by both anthropogenic (e.g., aerosol emissions and anthropogenic greenhouse gas) and natural (e.g., solar and volcanic activity) aspects. In contrast, simulations indicated by NAT were driven solely by natural factors. SSP245 was selected as the future projection in the study that extrapolates past and current global developments into the future based on moderate emission scenarios<sup>66</sup>.

### Estimation of flash drought evolution

SA is one of the significant hotspot regions where changing climate has amplified the risk of extreme weather events<sup>67</sup>. The summer monsoon rainfall is the key cause of surface water availability across many parts of SA;

however, it is well-documented that the drought's onset in SA is strongly interrelated with summer monsoon failure<sup>13</sup>. Thus, we aim to explore FD onset during the spring-summer transition season (March–August) and summer season (June–August), especially after the Kharif season (May–October). This is because Kharif crops are sown with the onset of the monsoon season in SA<sup>68–70</sup>. It is usually between June and July<sup>71</sup>. The fully-grown crops are harvested in the autumn, from September to October. We identified FD events based on the 5-day pentad mean of soil moisture percentile using the approach suggested by<sup>15,22</sup>. In this study, the methodology emphasizes the FD rapid intensification rate and the drought condition with a rapid decrease in soil moisture and the onset of drying. An FD event is identified when the 5-day pentad shows the soil moisture declining from more than the 40th percentile to less than the 20th percentile, with an average decrease rate of no less than 5% in soil moisture percentiles for each pentad. FD termination is considered when the declined soil moisture increases to the 20th percentile again. Notably, the 40th and 20th percentiles were estimated for each year during 1979–2021 using the same pentad to understand the relative changes in soil moisture at the same time each year. The FD onset speed is estimated as the average rate of reduction of soil moisture (between 20th to 40th percentiles) considering all pentad changes initiated from onset to termination periods of the FD episodes<sup>22</sup>.

As onset speed and intensification rate are the crucial aspects differentiating an FD from a conventional drought, we also closely investigated the FD's development after onset and intensity<sup>9</sup> and determined their seasonal changes during the spring-summer season. The intensification rate is estimated as the average rate of reduction of soil moisture (between 20<sup>th</sup> to 40<sup>th</sup> percentiles) considering all pentad changes initiated from onset to termination periods of the FD episodes<sup>22</sup>. The spring-summer intensity of FD is calculated as the mean soil moisture percentile of FD events over the spring-summer (March–August) months<sup>9,72</sup>. During the study, FD features (i.e., frequency, severity, and duration) are estimated based on the approach adopted by<sup>12,22,73</sup>. For instance, the FD frequency is calculated as the percentage of the number of pentads experiencing FD events in a given season (summer or spring-summer transition season). The FD duration is calculated as the average number of days that an event last. The severity of FD events is calculated as the accumulated mean soil moisture percentile deficits from the 40th percentile threshold until the termination of FD events. We used the same criteria adopted by<sup>15,22</sup> for the minimal duration of the FD episodes and eliminated those dry events that are no longer than 15 days (3-pentads) and, thus, have probably no impacts. Based on 1979–2021 climatology, the soil moisture percentile was determined for each grid point within the study area, and the average value across all grid-cells was estimated to represent the average percentile regionally. The FD onset speed for the spring-to-summer transition (referred to as spring-summer) is calculated as the change of regional averaged SM percentile from spring to summer (March to May percentile minus June to August percentile)<sup>9</sup>. This methodology is adopted by<sup>9</sup> for investigating the FD onset speed during the summer-autumn transition season in southern China.

### Estimation of joint return period

The Copula method<sup>74</sup> was applied to estimate the joint return period (JRP) of FD events in the historical period. The JRP was estimated to assess the combined distributions of FD duration and severity and their widespread influence on FD intensification. Here, we first determine the marginal distributions of FD severity and duration during the historical period under the umbrella of six distribution functions, i.e., Gamma, GEV, Weibull, Normal, Log-normal, and Inverse Gaussian, respectively. We then link the marginal distributions of FD severity and duration with the widely used copula families (i.e., Gaussian copula, Frank copula, and Gumbel copulas), and adopt only the best-fitting functions. The best-fitting copulas were determined based on the Akaike Information Criterion<sup>75</sup>. The best fitting copula function was employed with the ‘AND’ criterion to estimate bivariate probability distribution. For detailed methods of bivariate computation, readers are referred to prior studies<sup>36,74,76,77</sup>. Following the theory of Sklar's<sup>74</sup>, here the bivariate probability distribution e.g., duration and severity FD



( $d, s$ ) was articulated by its marginal distributions and the related dependence function:

$$FD(d, s) = C(FD_D(d), FD_S(s)) \quad (1)$$

where copula function signified with  $C$ , and  $FD_D(d)$  and  $FD_S(s)$  indicated the cumulative distribution functions for FD duration and severity, respectively. Similarly, the Frank, Gumbel, and Gaussian copulas are ranked as the bivariate candidate distributions<sup>78</sup>:

$$C_{Frank}(\theta) = -1 \frac{1}{\theta} \ln \left[ 1 + \frac{(e^{-\theta FD_D} - 1)(e^{-\theta FD_S} - 1)}{(e^{-\theta} - 1)} \right] (\theta \in [-\infty, \infty]) \quad (2)$$

$$C_{Gumbel}(\theta) = \text{Exp}\{-[(-\ln(FD_D))^\theta + (-\ln(FD_S))^\theta] / \theta\} (\theta \in [1, \infty]) \quad (3)$$

$$C_{Gaussian}(\theta) = \Phi_\theta(\Phi^{-1}(FD_D), \Phi^{-1}(FD_S)) (\theta \in [-1, 1]) \quad (4)$$

Under the copula family, numerous approaches of JRPs have been used in the recent past, for instance, the OR, AND, Kendall, and dynamic-based return periods<sup>74,77</sup>. Amongst them, the OR case ( $T_{or}$ ) is frequently implemented in drought and flood event assessment<sup>79</sup>:

$$T_{or} = \frac{E_I}{1 - FD(d, s)} = \frac{E_I}{1 - C[FD_D(d), FD_S(s)]} \quad (5)$$

where  $E_I$  symbolizes the estimated FD events inter-arrival time.

Under the bivariate framework, the appropriate choice of  $T_{or}$  attributes to vast combinations of FD events. The  $T_{or}$  can be obtained by the following mathematical equation:

$$\left\{ \begin{aligned} (d^*, s^*) &= \text{argmax } FD(d, s) = c[FD_D(d), FD_S(s)] f_D(d), f_S(s) \\ C(FD_D(d), FD_S(s)) &= 1 - E_I/T_{or} \end{aligned} \right\} \quad (6)$$

where the joint distributions of FD events denoted with  $FD(d, s)$ ,  $C[FD_D(d), FD_S(s)] = dC \frac{d(FD_D(d), s)}{d(FD_D(d))}$ ,  $d(FD_S(s))$  shows the copula density function, and  $FD_D(d)$  and  $FD_S(s)$  are joint distribution functions of FD duration and severity, respectively.

### Estimating fractional attributable risk

The ideal fraction of attributable risk (FAR) technique was adopted<sup>80</sup> to investigate the anthropogenic climate change influence on SA FD events. To do so, we first calculated the FD onset speed for the spring and summer seasons based on CMIP6 multi-model ensembled outputs using the ALL and NAT scenario for the period 1979–2021 across all grid-cells within the SA region. The change in FD onset speed during the spring-to-summer transition was estimated as the difference between the soil moisture percentile for the FD events during the spring and summer seasons (spring minus summer). Finally, FAR<sup>81,82</sup> for the change in FD onset speed was estimated to determine the influence of anthropogenic contributions on the spring-summer FD onset speed over SA. Mathematically, the FAR is expressed as follows:

$$FAR = \frac{FD_{ALL} - FD_{NAT}}{FD_{NAT}} \times 100 \quad (7)$$

where  $FD_{ALL}$  indicates the spring-summer FD onset speed estimated with the CMIP6 model ensembles in the ALL forcing,

### Data availability

All datasets used in the current study are freely accessible. Newly released CMIP6 models are publicly available via <https://esgf-node.llnl.gov/projects/>

[cmip6/](https://esgf-node.llnl.gov/projects/), and ERA5 climate datasets are freely available from <https://cds.climate.copernicus.eu/cdsapp#!/search?type=dataset>.

### Code availability

The Python code for flash drought estimation is available on request to the corresponding author.

Received: 14 October 2023; Accepted: 12 April 2024;

Published online: 20 May 2024

### References

- Pulwarty, R. S. & Sivakumar, M. V. K. Information systems in a changing climate: early warnings and drought risk management. *Weather Clim. Extrem.* **3**, 14–21 (2014).
- Mukherjee, S., Mishra, A. & Trenberth, K. E. Climate change and drought: a perspective on drought indices. *Curr. Clim. Chang. Reports* **4**, 145–163 (2018).
- Mishra, A. K. & Singh, V. P. A review of drought concepts. *J. Hydrol.* **391**, 202–216 (2010).
- Ullah, I. et al. Recent and projected changes in water scarcity and unprecedented drought events over Southern Pakistan. *Front. Earth Sci.* **11**, 1–16 (2023).
- Iyakaremye, V. et al. Increased high-temperature extremes and associated population exposure in Africa by the mid-21st century. *Sci. Total Environ.* **790**, 148162 (2021).
- Zou, R. et al. Characteristics and propagation of meteorological and hydrological droughts in eastern Gansu, a typical semi-arid region, China. *Int. J. Climatol.* **43**, 5327–5347 (2023).
- Svoboda, M. et al. The drought monitor. *Bull. Am. Meteorol. Soc.* **83**, 1181–1190 (2002).
- Nguyen, H. et al. Using the evaporative stress index to monitor flash drought in Australia. *Environ. Res. Lett.* **14**, 064016 (2019).
- Wang, Y. & Yuan, X. Anthropogenic speeding up of South China flash droughts as exemplified by the 2019 summer-autumn transition season. *Geophys. Res. Lett.* **48**, 1–9 (2021).
- Otkin, J. A. et al. Flash droughts: a review and assessment of the challenges imposed by rapid-onset droughts in the United States. *Bull. Am. Meteorol. Soc.* **99**, 911–919 (2018).
- Mukherjee, S., Mishra, A. K., Mann, M. E. & Raymond, C. Anthropogenic warming and population growth may double US heat stress by the late 21st century. *Earth's Futur.* **9**, 1–14 (2021).
- Mukherjee, S. & Mishra, A. K. Global flash drought analysis: uncertainties from indicators and datasets. *Earth's Futur.* **10**, 1–14 (2022).
- Mishra, V., Aadhar, S. & Mahto, S. Anthropogenic warming and intraseasonal summer monsoon variability amplify the risk of future flash droughts in India. *npj Clim. Atmos. Sci.* **4**, 1 (2021).
- Pendergrass, A. G. et al. Flash droughts present a new challenge for subseasonal-to-seasonal prediction. *Nat. Clim. Chang.* **10**, 191–199 (2020).
- Yuan, X. et al. Anthropogenic shift towards higher risk of flash drought over China. *Nat. Commun.* **10**, 1–8 (2019).
- Mahto, S. S. & Mishra, V. Dominance of summer monsoon flash droughts in India. *Environ. Res. Lett.* **15**, 104061 (2020).
- Christian, J. I. et al. Global distribution, trends, and drivers of flash drought occurrence. *Nat. Commun.* **12**, 6330 (2021).
- Mukherjee, S., Aadhar, S., Stone, D. & Mishra, V. Increase in extreme precipitation events under anthropogenic warming in India. *Weather Clim. Extrem.* **20**, 45–53 (2018).
- Iyakaremye, V. et al. Recent observed changes in extreme high-temperature events and associated meteorological conditions over Africa. *Int. J. Climatol.* **42**, 4522–4537 (2022).
- Sein, Z. M. M. et al. Observed spatiotemporal changes in air temperature, dew point temperature and relative humidity over Myanmar during 2001–2019. *Meteorol. Atmos. Phys.* **134**, 7 (2022).

21. Hu, C. et al. A new framework for the identification of flash drought: multivariable and probabilistic statistic perspectives: identification of flash drought. *Int. J. Climatol.* **41**, 5862–5878 (2021).
22. Mukherjee, S. & Mishra, A. K. A multivariate flash drought indicator for identifying global hotspots and associated climate controls. *Geophys. Res. Lett.* **49**, e2021GL096804 (2022).
23. Mukherjee, S. & Mishra, A. K. Increase in compound drought and heatwaves in a warming world. *Geophys. Res. Lett.* **48**, e2020GL090617 (2021).
24. Basara, J. B. et al. The evolution, propagation, and spread of flash drought in the Central United States during 2012. *Environ. Res. Lett.* **14**, 084025 (2019).
25. Zhang, Y., You, Q., Chen, C., Ge, J. & Adnan, M. Evaluation of downscaled CMIP5 Coupled with VIC model for flash drought simulation in a humid subtropical basin. *China. J. Clim.* **31**, 1075–1090 (2018).
26. Wang, Y. & Yuan, X. Land-atmosphere coupling speeds up flash drought onset. *Sci. Total Environ.* **851**, 158109 (2022).
27. Noguera, I., Vicente-Serrano, S. M. & Domínguez-Castro, F. The rise of atmospheric evaporative demand is increasing flash droughts in Spain during the warm season. *Geophys. Res. Lett.* **49**, 1–12 (2022).
28. Lisonbee, J., Woloszyn, M. & Skumanich, M. Making sense of flash drought: definitions, indicators, and where we go from here. *J. Appl. Serv. Climatol.* **2021**, 1–19 (2021).
29. Sein, Z. M. M. et al. Recent variability of sub-seasonal monsoon precipitation and its potential drivers in Myanmar using in-situ observation during 1981–2020. *Int. J. Climatol.* **42**, 3341–3359 (2022).
30. Saleem, F. et al. Population exposure changes to mean and extreme climate events over Pakistan and associated mechanisms. *GeoHealth* **7**, 1–17 (2023).
31. Liu, M. et al. Non-stationary frequency analysis of extreme streamflow disturbance in a typical ecological function reserve of China under a changing climate. *Ecohydrology* **23**, 1–20 (2021).
32. Ullah, I. et al. Spatiotemporal characteristics of meteorological drought variability and trends (1981–2020) over South Asia and the associated large-scale circulation patterns. *Clim. Dyn.* **60**, 2261–2284 (2023).
33. Nguyen, H., Wheeler, M. C., Hendon, H. H., Lim, E.-P. P. & Otkin, J. A. The 2019 flash droughts in subtropical eastern Australia and their association with large-scale climate drivers. *Weather Clim. Extrem.* **32**, 100321 (2021).
34. Mukherjee, S., Ashfaq, M. & Mishra, A. K. Compound drought and heatwaves at a global scale: the role of natural climate variability-associated synoptic patterns and land-surface energy budget anomalies. *J. Geophys. Res. Atmos.* **125**, 0–19 (2020).
35. Berg, A. et al. Impact of soil moisture–atmosphere interactions on surface temperature distribution. *J. Clim.* **27**, 7976–7993 (2014).
36. Ullah, I. et al. Projected changes in increased drought risks over South Asia under a warmer climate. *Earth's Futur.* **10**, 1–21 (2022).
37. Shahzaman, M. et al. Remote sensing indices for spatial monitoring of agricultural drought in South Asian countries. *Remote Sens.* **13**, 2059 (2021).
38. Aadhar, S. & Mishra, V. Increased drought risk in South Asia under warming climate: Implications of uncertainty in potential evapotranspiration estimates. *J. Hydrometeorol.* **21**, 2979–2996 (2020).
39. Ullah, R., Khan, J., Ullah, I., Khan, F. & Lee, Y. Investigating drought and flood evolution based on remote sensing data products over the Punjab region in Pakistan. *Remote Sens.* **15**, 1680 (2023).
40. Ullah, I. et al. Projected changes in socioeconomic exposure to heatwaves in South Asia under changing climate. *Earth's Futur.* **10**, 1–19 (2022).
41. Hina, S., Saleem, F., Arshad, A., Hina, A. & Ullah, I. Droughts over Pakistan: possible cycles, precursors and associated mechanisms. *Geomatics, Nat. Hazards Risk* **12**, 1638–1668 (2021).
42. Arshad, M. et al. Performance evaluation of ERA-5, JRA-55, MERRA-2, and CFS-2 reanalysis datasets, over diverse climate regions of Pakistan. *Weather Clim. Extrem.* **33**, 100373 (2021).
43. Nanditha, J. S. et al. The Pakistan flood of August 2022: causes and implications. *Earth's Futur.* **11**, e2022EF003230 (2023).
44. Aadhar, S. & Mishra, V. A substantial rise in the area and population affected by dryness in South Asia under 1.5 °C, 2.0 °C and 2.5 °C warmer worlds. *Environ. Res. Lett.* **14**, 114021 (2019).
45. Lange, S. et al. Projecting exposure to extreme climate impact events across six event categories and three spatial scales. *Earth's Futur.* **8**, 22 (2020).
46. Li, Q. et al. Different climate response persistence causes warming trend unevenness at continental scales. *Nat. Clim. Chang.* **12**, 343–349 (2022).
47. Ullah, I. et al. Evaluating the meteorological drought characteristics over Pakistan using in situ observations and reanalysis products. *Int. J. Climatol.* **41**, 4437–4459 (2021).
48. Trenberth, K. et al. Global warming and changes in drought. *Nat. Clim. Chang.* **4**, 17–22 (2014).
49. Qing, Y., Wang, S., Ancell, B. C. & Yang, Z. L. Accelerating flash droughts induced by the joint influence of soil moisture depletion and atmospheric aridity. *Nat. Commun.* **13**, 1139 (2022).
50. Latif, M., Syed, F. & Hannachi, A. Rainfall trends in the South Asian summer monsoon and its related large-scale dynamics with focus over Pakistan. *Clim. Dyn.* **48**, 3565–3581 (2017).
51. Preethi, B., Ramya, R., Patwardhan, S., Mujumdar, M. & Kripalani, R. Variability of Indian summer monsoon droughts in CMIP5 climate models. *Clim. Dyn.* **53**, 1937–1962 (2019).
52. Zhu, S. et al. Distinct impacts of spring soil moisture over the Indo-China peninsula on summer precipitation in the Yangtze river basin under different SST backgrounds. *Clim. Dyn.* **56**, 1895–1918 (2021).
53. Aadhar, S. & Mishra, V. On the occurrence of the worst drought in South Asia in the observed and future climate. *Environ. Res. Lett.* **16**, 024050 (2021).
54. He, C., Wang, Z., Zhou, T. & Li, T. Enhanced latent heating over the Tibetan plateau as a key to the enhanced east Asian summer monsoon circulation under a warming climate. *J. Clim.* **32**, 3373–3388 (2019).
55. Chen, X. & Zhou, T. Distinct effects of global mean warming and regional sea surface warming pattern on projected uncertainty in the South Asian summer monsoon. *Geophys. Res. Lett.* **42**, 9433–9439 (2015).
56. Shao, S., Zeng, X.-M., Wang, N., Ullah, I. & Lv, H. Attribution of Moisture Sources for Summer Precipitation in the Upstream Catchment of the Three Gorges Dam. *J. Hydrometeorol.* **25**, 353–369 (2024).
57. Mukherjee, S. & Mishra, A. K. Cascading effect of meteorological forcing on extreme precipitation events: Role of atmospheric rivers in southeastern US. *J. Hydrol.* **601**, 126641 (2021).
58. Mukherjee, S., Mishra, A. K., Zscheischler, J. & Entekhabi, D. Interaction between dry and hot extremes at a global scale using a cascade modeling framework. *Nat. Commun.* **14**, 277 (2023).
59. Kumar, S. et al. Terrestrial contribution to the heterogeneity in hydrological changes under global warming. *Water Resour. Res.* **52**, 3127–3142 (2016).
60. Seneviratne, S. I. et al. Investigating soil moisture–climate interactions in a changing climate: A review. *Earth-Science Rev* **99**, 125–161 (2010).
61. Schwingshackl, C., Hirschi, M. & Seneviratne, S. I. Quantifying spatiotemporal variations of soil moisture control on surface energy balance and near-surface air temperature. *J. Clim.* **30**, 7105–7124 (2017).
62. Lu, K. et al. Evaluating observed and future spatiotemporal changes in precipitation and temperature across China based on CMIP6-GCMs. *Int. J. Climatol.* **42**, 7703–7729 (2022).
63. Berg, A., Sheffield, J. & Milly, P. C. D. Divergent surface and total soil moisture projections under global warming. *Geophys. Res. Lett.* **44**, 236–244 (2017).
64. Hersbach, H. et al. Global reanalysis: goodbye ERA-Interim, hello ERA5. *ECMWF Newsl* **159**, 17–24 (2019).

65. Eyring, V. et al. Overview of the Coupled Model Intercomparison Project Phase 6 (CMIP6) experimental design and organization. *Geosci. Model Dev.* **9**, 1937–1958 (2016).
66. Neill, B. C. et al. The Scenario Model Intercomparison Project (ScenarioMIP) for CMIP6. *Geosci. Model Dev. Discuss.* <https://doi.org/10.5194/gmd-2016-84> **9**, (2016).
67. IPCC. *IPCC, 2021: AR6 WGI Technical Summary.* <https://doi.org/10.1017/9781009157896.002> 35–144 (2021).
68. Ullah, I. et al. Observed changes in seasonal drought characteristics and their possible potential drivers over Pakistan. *Int. J. Climatol.* **42**, 1576–1596 (2022).
69. Jha, R., Mondal, A., Devanand, A., Roxy, M. K. & Ghosh, S. Limited influence of irrigation on pre-monsoon heat stress in the Indo-Gangetic Plain. *Nat. Commun.* **13**, 4275 (2022).
70. Ullah, I. et al. Recent Changes in Drought Events over South Asia and Their Possible Linkages with Climatic and Dynamic Factors. *Remote Sens* **14**, 3219 (2022).
71. Laghari, A. N., Vanham, D. & Rauch, W. The Indus basin in the framework of current and future water resources management. *Hydrol. Earth Syst. Sci.* **16**, 1063–1083 (2012).
72. Ullah, I. et al. Future Amplification of Multivariate Risk of Compound Drought and Heatwave Events on South Asian Population. *Earth's Futur.* **11**, 1–16 (2023).
73. Yuan, X., Wang, L. & Wood, E. F. Anthropogenic Intensification of Southern African Flash Droughts as Exemplified by the 2015/16 Season. *Bull. Am. Meteorol. Soc.* **99**, S86–S90 (2018).
74. Salvadori, G., Durante, F., De Michele, C., Bernardi, M. & Petrella, L. A multivariate copula-based framework for dealing with hazard scenarios and failure probabilities. *Water Resour. Res.* **52**, 3701–3721 (2016).
75. Akaike, H. A new look at the statistical model identification. *IEEE Trans. Automat. Contr.* **19**, 716–723 (1974).
76. Shiau, J. T. Return period of bivariate distributed extreme hydrological events. *Stoch. Environ. Res. Risk Assess.* **17**, 42–57 (2003).
77. Sadeq, M. et al. Multihazard Scenarios for Analysis of Compound Extreme Events. *Geophys. Res. Lett.* **45**, 5470–5480 (2018).
78. Hintze, J. & Nelson, R. Violin Plots: A Box Plot-Density Trace Synergism. *Am. Stat.* **52**, 181–184 (1998).
79. Zhang, Q., Xiao, M. & Singh, V. P. Uncertainty evaluation of copula analysis of hydrological droughts in the East River basin, China. *Glob. Planet. Change* **129**, 1–9 (2015).
80. Allen, M. R. & Stott, P. A. Estimating signal amplitudes in optimal fingerprinting, part I: theory. *Clim. Dyn.* **21**, 477–491 (2003).
81. Stott, P. A., Stone, D. A. & Allen, M. R. Human contribution to the European heatwave of 2003. *Nature* **432**, 610–614 (2004).
82. Yuan, X. et al. A global transition to flash droughts under climate change. *Science (80-)* **380**, 187–191 (2023).

## Acknowledgements

The authors are thankful to the newly released Coupled Model Intercomparison Project Phase 6 (CMIP6) models institutions (listed in Supplementary Table 1 of this paper), European Centre for Medium-Range

Weather Forecasts Reanalysis 5 groups for development and making the datasets available to the scientific research community. We acknowledge the support of two Research Foundation- the National Natural Science Foundation of China for International Scientists (Grant No. 42350410438) and the China Postdoctoral Science Foundation (Grant No. 2023M730928), which enabled us to conduct this research.

## Author contributions

I.U. Conceptualization, Methodology, Formal analysis, Data curation, Visualization, Funding, Writing—original draft preparation: S.M. and A.K.M. Investigation and Writing—review and editing: S.S., S.A., and B.O.A. Writing—review and editing:

## Competing interests

The authors declare no competing interests.

## Additional information

**Supplementary information** The online version contains supplementary material available at <https://doi.org/10.1038/s43247-024-01390-y>.

**Correspondence** and requests for materials should be addressed to Irfan Ullah.

**Peer review information** *Communications Earth and Environment* thanks Ford Trenton and the other, anonymous, reviewer(s) for their contribution to the peer review of this work. Primary Handling Editors: Akintomide Akinsanola, Alireza Bahadori and Aliénor Lavergne. A peer review file is available.

**Reprints and permissions information** is available at <http://www.nature.com/reprints>

**Publisher's note** Springer Nature remains neutral with regard to jurisdictional claims in published maps and institutional affiliations.

**Open Access** This article is licensed under a Creative Commons Attribution 4.0 International License, which permits use, sharing, adaptation, distribution and reproduction in any medium or format, as long as you give appropriate credit to the original author(s) and the source, provide a link to the Creative Commons licence, and indicate if changes were made. The images or other third party material in this article are included in the article's Creative Commons licence, unless indicated otherwise in a credit line to the material. If material is not included in the article's Creative Commons licence and your intended use is not permitted by statutory regulation or exceeds the permitted use, you will need to obtain permission directly from the copyright holder. To view a copy of this licence, visit <http://creativecommons.org/licenses/by/4.0/>.

© The Author(s) 2024